Journal of Atmospheric and Solar-Terrestrial Physics 118 (2014) 2–15

Contents lists available at ScienceDirect

Journal of Atmospheric and Solar-Terrestrial Physics

journal homepage: www.elsevier.com/locate/jastp

Program of the Antarctic Syowa MST/IS radar (PANSY)

Kaoru Sato [a,*], Masaki Tsutsumi [b], Toru Sato [c], Takuji Nakamura [b], Akinori Saito [d], Yoshihiro Tomikawa [b], Koji Nishimura [b], Masashi Kohma [a], Hisao Yamagishi [b], Takashi Yamanouchi [b]

[a] Department of Earth and Planetary Science, The University of Tokyo, Japan
[b] National Institute of Polar Research, Japan
[c] Department of Communications and Computer Engineering, Kyoto University, Japan
[d] Department of Geophysics, Kyoto University, Japan

ARTICLE INFO

Article history:
Received 4 January 2013
Received in revised form
12 July 2013
Accepted 26 August 2013
Available online 31 August 2013

Keywords:
MST radar
Antarctic atmosphere
Polar lows
Polar stratospheric clouds
Polar mesospheric clouds
Gravity waves
Tides
Turbulence
Tropopause
Ozone hole
Stratosphere
Mesosphere
Ionosphere
Polar mesosphere summer echo
The PANSY radar

ABSTRACT

The PANSY radar is the first Mesosphere–Stratosphere–Troposphere/Incoherent Scatter (MST/IS) radar in the Antarctic region. It is a large VHF monostatic pulse Doppler radar operating at 47 MHz, consisting of an active phased array of 1045 Yagi antennas and an equivalent number of transmit–receive (TR) modules with a total peak output power of 500 kW. The first stage of the radar was installed at Syowa Station (69°00′S, 39°35′E) in early 2011, and is currently operating with 228 antennas and modules. This paper reports the project's scientific objectives, technical descriptions, and the preliminary results of observations made to date. The radar is designed to clarify the role of atmospheric gravity waves at high latitudes in the momentum budget of the global circulation in the troposphere, stratosphere and mesosphere, and to explore the dynamical aspects of unique polar phenomena such as polar mesospheric clouds (PMC) and polar stratospheric clouds (PSC). The katabatic winds as a branch of Antarctic tropospheric circulation and as an important source of gravity waves are also of special interest. Moreover, strong and sporadic energy inputs from the magnetosphere by energetic particles and field-aligned currents can be quantitatively assessed by the broad height coverage of the radar which extends from the lower troposphere to the upper ionosphere. From engineering points of view, the radar had to overcome restrictions related to the severe environments of Antarctic research, such as very strong winds, limited power availability, short construction periods, and limited manpower availability. We resolved these problems through the adoption of specially designed class-E amplifiers, light weight and tough antenna elements, and versatile antenna arrangements. Although the radar is currently operating with only about a quarter of its full designed system components, we have already obtained interesting results on the Antarctic troposphere, stratosphere and mesosphere, such as gravity waves, multiple tropopauses associated with a severe snow storm in the troposphere and stratosphere, and polar mesosphere summer echoes (PMSE).

1. Introduction

The polar regions play an important role in the Earth's climate system. They are in the downward branches of the material circulation in the troposphere and stratosphere, and in the upward (downward) branch during the summer (winter) in the mesosphere. This material circulation in the middle atmosphere is essentially wave-driven and maintains its thermal structure far from that which could be expected by radiative balance alone. The resulting low temperature in the summer upper mesosphere leads to conditions under which polar mesospheric clouds (PMC) form, and low temperature in the polar winter is confined solely to the lower stratosphere where polar stratospheric clouds (PSC) form. PSC serve as an environment for producing the conditions that can lead to catalytic destruction of ozone during Antarctic spring, and are considered responsible for forming the ozone hole. PMC are a phenomenon also known as noctilucent clouds that were first reported late in the 19th century a few years after the Krakatoa volcanic eruption. Although those PMC may have first appeared accidentally as a result of the water vapor and aerosols injected into the atmosphere by the volcanic eruption, they have been observed continuously since then. PMC have even been observed recently at mid-latitudes, such as those observed over Paris in the summer of 2009, which are still fresh in our memory. The occurrence frequency of PMC exhibits interannual variability, and

* Correspondence to: Department of Earth and Planetary Science, The University of Tokyo, 7-3-1 Hongo, Bunkyo-ku, Tokyo 113-0033, Japan. Tel.: +81 3 3814 7549.
E-mail address: kaoru@eps.s.u-tokyo.ac.jp (K. Sato).

1364-6826/$ - see front matter © 2013 Elsevier Ltd. All rights reserved.
http://dx.doi.org/10.1016/j.jastp.2013.08.022

particularly susceptible to solar cycle modifications (von Zahn, 2003). However simultaneously it seems that there is a trend in the PMC occurrence frequency that is likely due to increases in water vapor originating from the methane and the radiative cooling caused by the increase in the carbon dioxide (CO_2) emitted as a result of human activity (Thomas et al., 2003). Thus, PMC are sometimes called "the canaries in a coal mine" of the Earth climate system. Therefore, the monitoring and study of these phenomena are important tools in detecting climate change, and thus in understanding the Earth climate system. Strong echoes called polar mesosphere summer echoes (PMSE) which are frequently associated with PMC are detected by mesosphere observations during summer via various kinds of radars operating at frequencies ranging from a few MHz to several hundred MHz (Cho and Roettger, 1997; Rapp and Luebken, 2004).

Another interesting polar phenomenon is the high albedo and high elevation of the Antarctic continent, which can cause strong downslope (katabatic) winds in the coastal region. These winds are an important source of gravity waves in the Antarctic. Moreover, the polar atmosphere is different from lower latitude regions because of strong and sporadic energy inputs from the magnetosphere by energetic particles and field-aligned currents.

Despite the importance of the southern polar atmosphere, observational studies have thus far been restricted due to the harsh physical conditions of the Antarctic continent. In order to address this deficiency, to explore the physics of these unique phenomena, and to study the quantitative effects of the polar atmosphere on the Earth's climate, a Mesosphere–Stratosphere–Troposphere/Incoherent Scatter (MST/IS) radar (a VHF clear-air Doppler radar) has been installed at Syowa Station (69°S, 40°E) in early 2011; the first of its kind in the Antarctic. This radar has been named PANSY after the name of the project itself. A "pansy" is a type of flower, and its name derives from the French word "*penser*" which means "to think".

Although the term "MST radar" does not have a concrete definition, it has been used to define a system having sufficiently higher sensitivity than Stratosphere–Troposphere (ST) radars, whose coverage is limited to the troposphere and stratosphere (e.g., Gage and Balsley, 1978; Bowhill, 1983). The average-power-aperture product for such a system is more than 10^8 W m^2, a typical example being that of the MU radar (4×10^8 W m^2) located in Shigaraki, Shiga, Japan (Fukao et al., 1985). While existing 50 MHz radars in Antarctica (Morris et al., 2004; Kirkwood et al., 2007) also detect enhanced echoes in the mesospheric region such as meteor-trail echoes, and enhanced echoes which are specific for polar regions such as PMSE and Polar Mesosphere Winter Echoes (PMWE), they are not powerful enough to be considered true MST radars.

The first stage of the radar construction at Syowa Station began in December 2010 and was completed in March 2011. The first tropospheric test observations were conducted utilizing a small system consisting of 57 Yagi antennas (out of the 1045 planned for the full system) and an equivalent number of transmit–receive (TR) modules on March 31, 2011. Clear air echoes were observed at altitudes up to about 6 km, and wind velocity was estimated, which showed good agreement with that from observations by radiosondes launched from Syowa Station.

During the Antarctic winter of 2011, however, the level of snow falling at Syowa Station was the highest recorded since monitoring began in 1956, and many antennas were buried under snow. While the antenna elements were severely damaged due to the weight of the accumulated snow, the radar system itself, including TR modules mounted on the antenna masts, suffered only minor damage. As a result, in January and February 2012, continuous PMSE observations were successfully conducted with 19 antennas that escaped serious damage.

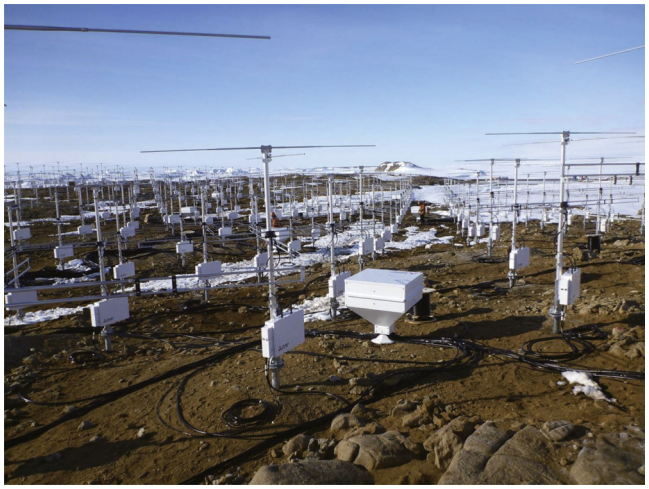

Fig. 1. Field view of the antenna system of the PANSY radar taken during the second stage of construction.

Table 1
Basic parameters of the PANSY radar.

System	Pulse Doppler radar Active phased array system
Center frequency	47 MHz
Antenna	An irregular array consisting of 1045 crossed Yagi antennas Effective diameter about 160 m (18,000 m^2)
Transmitter	1045 Solid-state TR modules Peak Power: 520 kW
Receiver	(55+8) Channel digital receiving systems Ability of imaging and interferometry observations
Peripheral	24 Antennas for E-layer FAI observation

The second stage of construction was started in December 2011, and was completed in March 2012. While the original plan called for the installation of 532 TR modules in order to begin observations with a half-system, the icebreaker ship Shirase was, unfortunately, unable to reach Syowa Station due to extra-ordinarily thick offshore ice, and we were only able to transfer about 40% of our equipment consignment to the station. Despite this setback, the emplacement of 228 antennas and accompanying TR modules was completed, and the first continuous observation with this partial system started on March 7, 2012. Fig. 1 shows a part of the antenna system erected during this stage of construction.

In this paper, we will present an overview of the radar system, the scientific targets of the PANSY radar, and preliminary results of observations made with this system.

2. Radar system

2.1. General technical description

The PANSY radar is a monostatic pulse Doppler radar operating at 47 MHz. Its antenna is an active phased array consisting of 1045 three-element crossed Yagi antennas in its final system. The beam direction can be pointed to any specified direction within 30° of the zenith. Each of the 1045 antennas is equipped with a solid-state TR module with 500 W peak output power, and the total output power is 520 kW. The fundamental parameters of the radar are given in Table 1.

The basic concept of the PANSY radar system calls for a sensitivity level comparable to that of the MU radar, which covers a height region of 1.5–600 km (Fukao et al., 1985). One of the major technical limitations in designing the PANSY radar is its

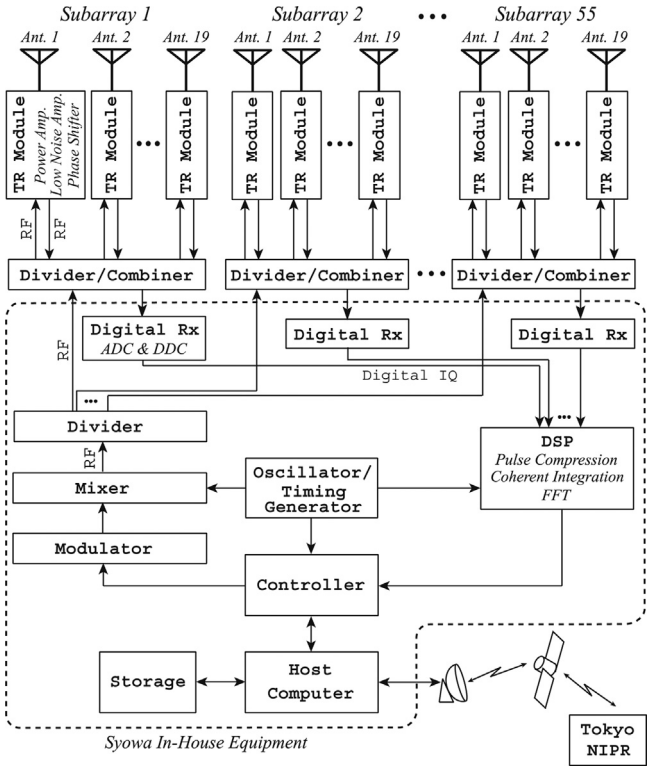

Fig. 2. General block diagram of the PANSY radar. Components enclosed by a dashed line are located in the operations building next to the antenna area.

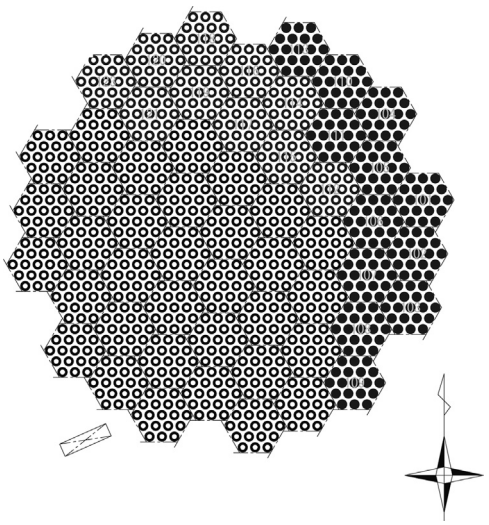

Fig. 3. Arrangement of the original (circular) array. Black dots indicate the 12 TR module subarrays currently in operation. Each hexagon denotes a subarray of 19 crossed Yagi antennas. The rectangle indicates the radar operations building.

power consumption. While the MU radar with its class-AB power amplifier consumes 230 kW, the maximum available power for the PANSY radar at Syowa Station is less than 100 kW. Since the product of the total output power and the antenna's effective area determines the sensitivity of an atmospheric radar system, we reduced the output power to half of that of the MU radar, and doubled the antenna area. In order to further reduce the power consumption, we developed a new class-E amplifier with a total power efficiency exceeding 50%. As a result, we were able to achieve a total power consumption of 75 kW, which includes the power needed for the digital signal processing system. This power-efficient design enabled us to avoid the use of a cooling fan, thus resulting in a robust TR module without any moving components, which is ideal for the long-term operation in the severe weather conditions in Antarctica. It has been confirmed that the modules can be continuously operated during the winter, even when fully buried under snow.

Fig. 2 shows a general block diagram of the radar system. The transmitted pulses are generated, coded, converted to radio frequency (RF) of 47 MHz, and divided into 55 channels, which correspond to 55 antenna subarrays, in the operations building located next to the antenna area. Components located in the operations building are enclosed by a dashed line in the block diagram. From the operations building, cables for the RF signal, the control signal, and the DC power supply extrude out to the 55 divider/combiner modules located near the center of each antenna subarray. Next, the signals are further divided into the hexagonal-shaped subarrays consisting of 19 antennas each, and then fed to the TR module mounted on each antenna mast. Each TR module consists of a class-E power amplifier, a TR switch, a 90° hybrid used to excite two orthogonal Yagi's for circular polarization, a low-noise pre-amplifier, and an 8-bit phase shifter.

The received signal is processed by an array of 55 digital receivers, which directly samples the RF signals and converts them into the baseband IQ signals. Each antenna subarray is connected separately to a digital receiver, so that imaging observations of atmospheric turbulence, as well as the ionospheric irregularities can be performed. The data is processed in the digital signal-processing unit for pulse decompression, coherent integration, and Fast Fourier Transform (FFT) operations in order to obtain the echo power spectra.

Another important design issue was (and is) the construction of the radar at Syowa Station in the Antarctic, which must be performed during the short 2-month summer period by untrained members of the Antarctic research expedition—most of whom are scientists (not technicians). Additionally, since the Antarctic Treaty forbids major alterations to virgin ground, the use of heavy construction vehicles is likewise prohibited. Because of these restrictions, we minimized the weight of the antennas and the TR modules to the greatest extent possible. Furthermore, the three-element crossed Yagi antennas had to be able to withstand maximum continuous wind speeds of up to 65 m s^{-1}. After examining several test antennas at Syowa Station, we settled on the current design, which has a weight of 12 kg. The Yagi antenna used for each polarization has an isotropic gain of 7.2 dB, a bandwidth of 2 MHz centered at 47 MHz, and a voltage standing wave ratio (VSWR) of less than 1.25 in this band. Its half-power beam width is 68° in the E-plane, and 126° in the H-plane.

The TR module was also designed to have minimum cross-section and weight (18 kg). During installation, the supporting mast (to which the antenna along with the TR module is attached) is inserted into a 130-mm-diameter and 1-m-deep mounting hole. The height of each antenna can be varied in a range of approximately 2 m to conform to ground surface conditions, and the phase of the radiated signal is electronically adjusted to compensate for the height difference. The antennas are arranged to form a grid of equilateral triangles with 4.5 m intervals, which corresponds to 0.7 the wavelength. As previously mentioned, each hexagonal shaped subarray consists of 19 antennas, so the entire antenna array will consist of 55 hexagonal subarrays when completely assembled.

The arrangement of these 55 subarrays was originally designed to form a quasi-circular shape 160 m in diameter, as shown in Fig. 3. However, as stated above, we experienced an extremely heavy snowfall at Syowa Station during the Antarctic winter of 2011. As the dominant wind direction at Syowa Station is from the northeast, the effect of snow was especially notable at the central and southwestern regions of the planned antenna area, where the

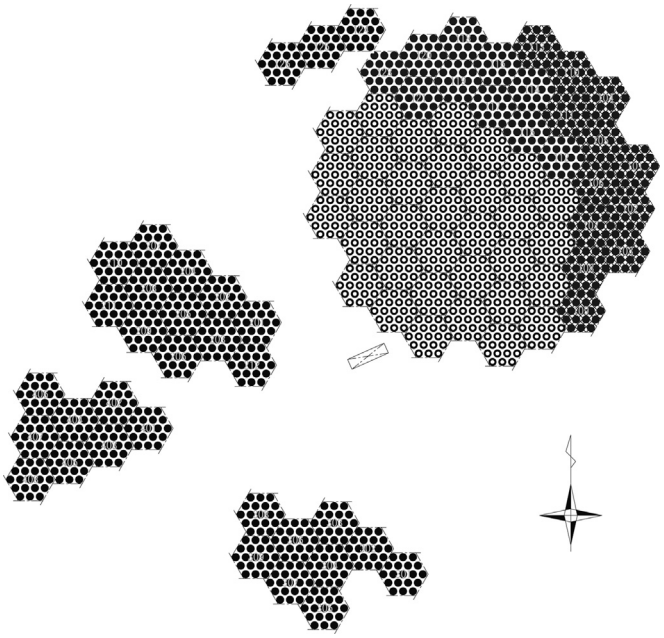

Fig. 4. Same as Fig. 3, but for the arrangement of relocated antennas (upper right part of the circular array plus four attached blocks).

maximum snow level exceeded 3 m. After examining the snow record during the winter, we selected four blocks of hilly areas near the original array, where snow levels were relatively low, and moved a portion of the antennas into these areas during the summer operation from December 2011 to February 2012. Fig. 4 shows the arrangement of the relocated antennas. Currently, the TR modules are mounted in 12 antenna subarrays located at the upper right part of the array, as indicated by the black dots in Fig. 3.

The basic idea behind this relocation was to retain the hexagonal shape of each subarray consisting of 19 crossed Yagi antennas, and to concentrate the subarrays as tightly as possible, while avoiding areas prone to deep snow. The size of the entire modified antenna area eventually became about 320 m in diameter, which is twice the original planned size. This enlargement had the twofold effects of sharpening of the mainlobe and increasing the sidelobe level. It should be noted that the overall sensitivity of the system remained unchanged from the original plan because the total number of antennas remained the same.

Fig. 5a shows the computed two-way beam pattern of the rearranged version of the full antenna array with uniform excitation. In this computation, we first calculate the element antenna pattern of a crossed Yagi antenna placed on a planar ground with the method-of-moment. As the three-dimensional (3D) position of all antenna elements are precisely measured during

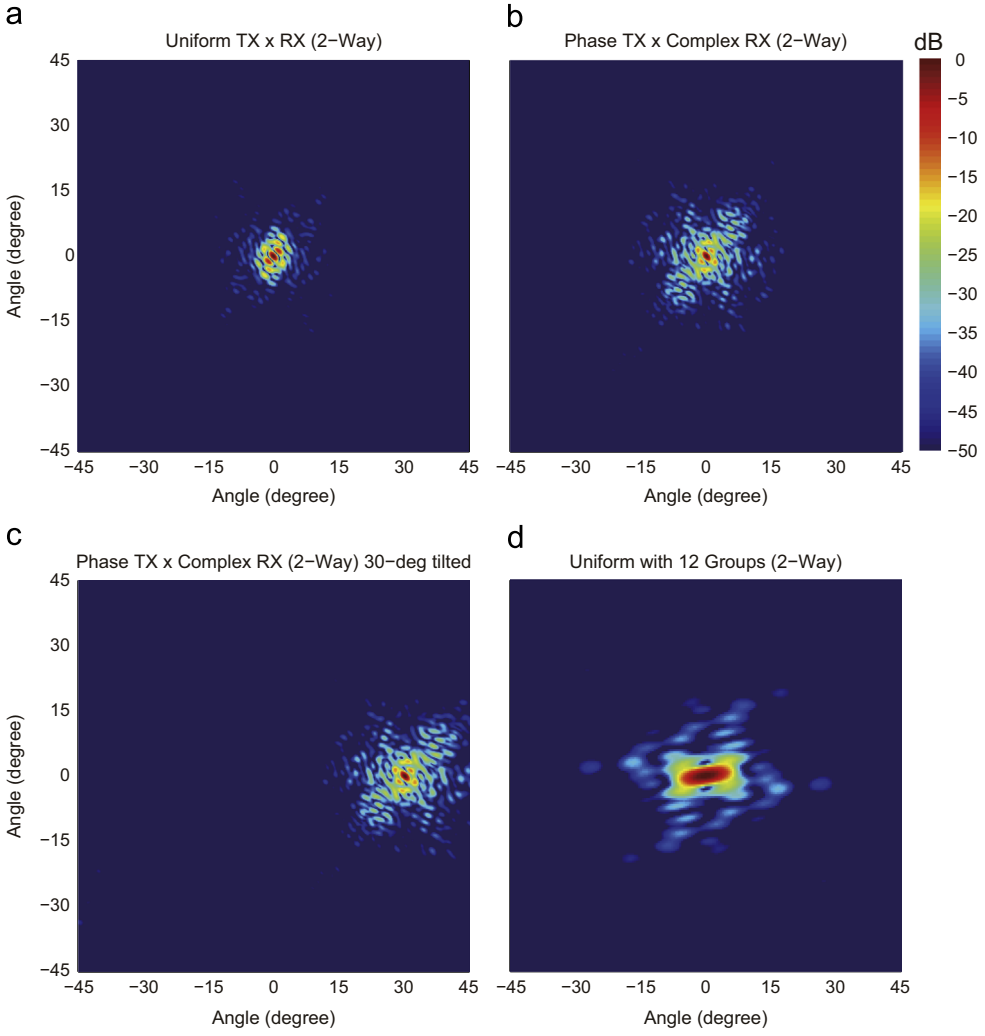

Fig. 5. Computed two-way antenna pattern of the rearranged array with (a) uniform excitation for both transmission and reception, and (b) with an optimization of phase in transmission plus phase and amplitude in reception. Figure (c) is same as (b), but for a case where the mainlobe is tilted 30° from the zenith. Figure (d) shows the beam pattern for the existing 12 subarrays shown in Fig. 3.

the construction process, we can accurately synthesize the antenna pattern in the far field by summing the contribution from all elements while taking the path difference into account. It is also necessary to consider the two-way beam pattern because the contributions of scattering from the sidelobe regions should be measured by their weight in the received echo power, which is determined by the product of the transmission and reception beam patterns. In this figure, since we use the same pattern for both transmission and reception, the one-way pattern can be easily obtained by dividing the dB number in the contour scale by two.

Although the half-power width of the mainlobe is sharpened to about 1°, compared to 2.2° for a 160-m-diameter circular array, the maximum sidelobe level reaches −7.5 dB from the mainlobe level in the two-way pattern. Since this level is too high to allow us to disregard the contributions of sidelobe echoes, it is not fair to simply evaluate the beam width at its half-power level. One of the important effects of a finite beam width in atmospheric radar applications is the beam broadening effect on determining the spectral width, which is a measure of the turbulence intensity (e.g., Hocking, 1985). In this regard, the effect of the finite beam width is measured by the second order moment of the Doppler spectrum. A rough measure of the lower limit, below which contributions can be safely neglected, may be −10 dB from the peak. An effective beam width that includes the contribution of these very high sidelobes measured at −10 dB level is about 4.0°, with slight variations along the azimuth direction.

In order to reduce the sidelobe level, we plan to optimize the phase and amplitude of each antenna module. Fig. 5b shows an example of such an attempt. When transmitting, all antennas are excited with uniform amplitude and controlled phase because we are unable to change the amplitude of each transmitter. On reception, both the amplitude and phase of all elements are controlled. To accomplish this, we employed a simulated annealing algorithm commonly used for optimization problems (Kirkpatrick et al., 1983). Based on the results of our calculations, the maximum sidelobe level was reduced to −13.5 dB, which is tolerable for most atmospheric observations. In this case, the cost of this reduction is the loss of sensitivity of about 6 dB, due to non-uniform amplitude and phase when combining the signals of all modules. Fig. 5c shows the same beam pattern as in Fig. 5b, but for a case when the mainlobe is tilted 30° from the zenith. Although the external shape of the array is irregular, all antenna elements are placed on a regular equilateral triangular grid with 0.7 wavelength spacing. For this grid arrangement, grating lobes appear only when the mainlobe is tilted more than 41° from the zenith, and thus we can safely steer the antenna beam up to 30° from the zenith to any azimuthal direction. Fig. 5d shows the beam pattern for the existing 12 subarrays shown in Fig. 3.

Conventional uniform excitation will be used primarily for observations that require maximum sensitivity, such as the lower stratosphere, mesosphere, and ionosphere. The optimized pattern will be especially effective during imaging observations for which sharp beams are essential. We will further investigate algorithms to determine which provide a better compromise between sidelobe suppression and loss of sensitivity. In addition, we intend to continue monitoring the snow levels, and to move some of the antenna subarrays back into the central region of the original array if conditions allow.

2.2. Tropo/stratosphere observation

The transmitted pulse length is variable but has a minimum length of 0.5 μs, corresponding to a height resolution of 75 m. In order to increase sensitivity, Spano codes (Spano and Ghebrebrhan, 1996), which are an extension of complementary codes, are employed.

When applying the pulse compression, the nonlinear nature of the class-E amplifier causes a serious problem. Binary phase pulse compression schemes postulate the linear response of the transmitter. More specifically, the output to the pulse codes are expressed as superposition of that for a single pulse shifted in time and multiplied by +1 or −1 in amplitude. Unfortunately, the class-E amplifier has a different response time at the leading and trailing edges of the outer envelope of pulse trains, the latter being slightly longer than the former. This nature was partly mitigated by pre-distorting the input waveform of the power amplifier, but not to the −30 dB suppression level required for the code sidelobes. In order to solve this problem, we separated each bit of the pulse code in time, thus creating a train of pulses with an interval equal to the pulse length.

The antenna beam direction can be switched by electronically controlling the phase of each antenna module for each transmitted pulse. The basic observation scheme for the troposphere and stratosphere is five beam directions (vertical, north, east, south, and west with zenith angle of 10°). The beam direction is switched at each pulse to prevent range-aliased echoes. Other observation parameters currently used include the following: 1 μs sub-pulse with 16-bit Spano codes, 400 μs inter pulse period (IPP), 64 coherent integrations, 128-point FFT, and seven incoherent integrations. The total time resolution is 115 s.

Atmospheric radar backscattering is caused by fluctuations in the refractive index of the air. More precisely, such backscattering is the Bragg scattering from the wavenumber component of the fluctuations that are half the radar wavelength (3.2 m for the PANSY radar). The main contributor to fluctuations in the lower and middle atmosphere index of refraction is disturbances in the background gradient of air density with height caused by atmospheric turbulence. Fluctuations in water vapor also play an important role in the lower troposphere. In addition to the background wind, the intensity of the atmospheric turbulence can be measured in this height region. As air density declines exponentially with height, the fluctuations, (and thus the echo power,) also decline. The mean lapse rate of the echo power in the mid-latitude lower stratosphere is about 2–3 dB km^{-1}.

If we assume that the turbulence intensity is the same, the maximum observation height of an atmospheric radar in the stratosphere is determined by the antenna effective area, average transmitter power, and the required height and time resolutions. As the power-aperture product of the PANSY radar is approximately the same as that of the MU radar, it is expected that these two radars have similar maximum observation height under the same observation condition. The maximum observation height of the MU radar, with 150-m height resolution and 30-min time resolution, is about 24 km (Sato et al., 1997).

2.3. Mesosphere observation

Ionization becomes the major contribution to the refractive index above about 50 km. The advantage of using the lower VHF band is that the turbulent eddies still have substantial magnitude at the size of half the radar wavelength at mesospheric heights. In the low- and mid-latitude regions, coherent scattering echoes, which are considered to come from refractive index gradient of the ionization enhanced by atmospheric turbulence, have been observed in the daytime mesosphere of 60–80 km (e.g., Fukao et al., 1979; Roettger et al., 1979; Sato et al., 1985). We expect to detect these echoes during daytime hours by the PANSY radar when the system is fully operational. As described in the following section, enhanced coherent echoes, PMSE, are also observed during the summer season. Enhanced echoes, PMWE, are also observed in the winter (e.g., Morris et al., 2011). Although the

PANSY radar has already confirmed the occurrence of this type of echoes, detailed analysis will be the subject of future work.

The basic observation parameters of the mesosphere are similar to those for tropo/stratosphere observation, but with a longer sub-pulse of 4 μs utilized in order to detect weaker echoes at a cost of a lower height resolution of 600 m.

2.4. Ionosphere observation

From altitudes of about 100 km to about 500 km, incoherent scattering by ionospheric electrons can be observed via the PANSY radar. Electron and ion density, their temperatures, and the ion drift velocity, are derived by analyzing the echo power spectra. As the nature of incoherent scatter is quite different from the coherent scatter in the lower regions, and is characterized by a much shorter coherence time, ionospheric observations require the use of special observation mode. Accordingly, we intend to follow the observation setup and parameters developed by Sato et al. (1989) for the incoherent scatter observations with the MU radar. The basic observation modes are: the electron density profile mode using sub-pulse of 32 μs with 13-bit Barker code, the ion and electron temperature mode with 3- or 4-pulse sequences to measure the auto-correlation function (ACF) of the ion component of incoherent scatter, and the ion drift mode with a double pulse scheme to determine Doppler shift from a single ACF lag. These modes usually require incoherent integration of over 10–60 min to detect very weak incoherent scatter echoes. Real-time identification and rejection of meteor echoes and space debris echoes is essential, and was also developed by Sato et al. (1989).

One special nature of the Antarctic VHF radar is the existence of strong coherent echoes due to ionospheric field-aligned irregularities (FAI) of auroral origin. These echoes are observed in a direction perpendicular to the Earth's magnetic field, which has an inclination angle of about 70° near Syowa Station. As the main antenna array cannot be pointed to an elevation angle of 20°, a peripheral array consisting of 24 Yagi antennas set to this angle is used for this purpose. The Yagi antennas used for this array are identical to those used for the main array, except that only horizontal polarization is excited. The output of the array can be connected to each of eight digital receivers dedicated to the FAI observations. The same peripheral array will be used to suppress the possible interference of FAI echoes on the weak incoherent scatter echoes observed by the main array. A special adaptive antenna algorithm will be developed to cope with this problem.

2.5. Meteor observation

MST radars have also been used for a variety of observations based on meteor echo measurements. Specular echoes scattered by ionized meteor trails are detected in the altitude region of 75–105 km, and in the horizontal range within a few hundred kilometers. These echoes have been intensively observed using the MU radar for the study of atmospheric dynamics (e.g. Nakamura et al., 1991). The Doppler frequency shifts and exponential power decay in these echoes provide information of horizontal wind velocities and ambipolar diffusion, respectively. The latter is further used to extract temperature fluctuations caused by atmospheric waves (Tsutsumi et al., 1994, 1996; Nakamura et al., 1997). Trail echo observations by PANSY have two major advantages over conventional meteor radar observations. First, the 500 kW transmitting power is one to two orders larger. Second, a post beam steering technique can be applied to the unprecedented number of 55 receiver signals, each of which is obtained from one antenna selected from individual antenna subarrays. The sharp receiving beam can detect very faint meteor echoes that are never seen in a single receiver output. The number of echoes is expected to be at least 10 times more than that of traditional meteor radars and can further enable resolution of the horizontal structure of wind and temperature fields by splitting the scattering volume into small sections and estimating those parameters in each of them. This advanced meteor observation technique will be especially useful when used to compensate for turbulence echo observations in the mesosphere, which require ionization, that is, solar radiation and are thus very hard to conduct during the long polar night.

Another important meteor based target is meteor head echoes. With the high transmitting power concentrated in the sharp beam and multiple digital receiver channels, PANSY can measure meteoroid range, orientation, impinging velocity and deceleration, and thus the precise orbital information, very accurately using the techniques that have been developed based on MU radar observations (Sato et al., 2000; Nishimura et al., 2001; Kero et al., 2012).

3. Scientific targets

The basic observation mode of the PANSY radar for the neutral atmosphere provides vertical profiles of three-dimensional (3D) wind vectors over a wide height range in the troposphere, stratosphere and mesosphere. Vertical resolution is 75 m at best, but is usually 150 m for the troposphere and stratosphere and 600 m for the mesosphere. Horizontal resolutions corresponding to the half-power beam width of 1° are 300 m at the height of 20 km and 1.2 km at 75 km. It should be noted that the vertical resolution for the beams tilted to 10° and 30° from the zenith is increased by 17% and 50%, respectively, of the horizontal resolution. For the studies of wave structures, the horizontal separation of oblique beams is the major limiting factor determining the minimum detectable horizontal scale. Various atmospheric phenomena and dynamical processes are examined by continuous observations with the fine vertical and horizontal resolutions. These include polar lows causing severe snow storms, tropospheric circulation associated with katabatic winds, fine structure of the tropopause, stratopause and mesopause, sudden stratospheric warming, polar vortex break-up, medium-scale Rossby waves trapped at the edge of the polar vortex, dynamics of PSC and PMC, atmospheric turbulence, and atmospheric gravity waves. The response of the neutral atmosphere to the energy inputs from the magnetosphere is also an important topic of the PANSY project.

3.1. Tropospheric phenomena: katabatic wind and cyclones

The coastal region of the Antarctic continent frequently suffers from severe snow storms, except for a quite short time period of December and January in the summer (Sato and Hirasawa, 2007). It is considered likely that such severe snow storms are related to mesoscale cyclones, and are reinforced by katabatic flows along the coastal slope. However, the cyclogenesis mechanism and interaction between the cyclones and katabatic flows remains somewhat unclear (e.g., Bromwich et al., 2011). The severe weather is not simply due to confluence of strong winds from the two systems, but is also due to other effects unique to the Antarctic region, such as a lee trough formed by advection of high potential temperature air from the continent by katabatic winds, and baroclinic instability due to the strong horizontal gradient of sensible and latent heat fluxes on the peripheral sea ice, whose distribution is affected by katabatic winds. To elucidate its quantitative nature, coordinated studies using numerical models and observations with similarly high resolutions are needed. MST radars, such as the PANSY radar can provide fine resolution observational data, including horizontal and vertical winds, which meets those requirements.

3.2. Atmospheric gravity waves in the troposphere, stratosphere and mesosphere

The spectra of atmospheric gravity waves are distributed over a wide range of frequency, and horizontal and vertical wavenumbers. Consequently, it is usually impossible to observe the whole gravity wave continuum using a single instrument because of the observational filter problem (Alexander et al., 2010). Continuous observation with fine temporal resolution at one location using an MST radar allows us to extract gravity wave components by their high frequency nature using a time filter. The horizontal and vertical resolution of an MST radar is sufficiently high to detect gravity waves, even those with small horizontal and vertical scales. Thus, it can observe gravity waves in almost all horizontal and vertical wavenumber ranges if they have high ground-based frequencies, which covers a part of the spectral range that is invisible to conventional radiosondes and recent high-resolution satellite observations. Moreover, the ground-based frequency is conserved during wave propagation if the background field is steady. Since the mean wind usually has vertical shear, the conservation of frequency is a reasonable assumption compared with that of the vertical wavenumber. Thus, the wave force can be estimated by using the vertical profile of the momentum fluxes associated with gravity waves observed by an MST radar. Furthermore, direct and accurate estimates of the momentum flux vector associated with atmospheric gravity waves are possible using the dual beam method (Vincent and Reid, 1983).

According to the gravity wave study by Yoshiki and Sato (2000) using operational radiosonde data, the characteristics of the atmospheric gravity waves at Syowa Station are similar to those at other Antarctic stations, such as the spring maximum observed in the gravity wave activity. Thus, it is expected that the nature of the waves observed by the PANSY radar will be typical of others observed in the Antarctic, despite the fact that observations are only taken at a single location. Recent works using high-resolution satellite observations (Ern et al., 2004; Alexander et al., 2008) and a gravity-wave resolving general circulation model (Watanabe et al., 2008; Sato et al., 2009, 2012) show that gravity waves have large energy in the high latitude regions of the Southern Hemisphere in austral winter (Geller et al., in press). Moreover, the lateral propagation of gravity waves toward the mesospheric westerly jet around 60°S (Sato et al., 2009) and/or upward propagation of gravity waves excited over small islands in the Antarctic Sea (Alexander et al., 2009), neither of which have been parameterized in climate models, may largely improve a significant model bias in the timing of the Antarctic ozone hole disappearance in summer (McLandress et al., 2012). The generation and propagation of such gravity waves, as well as their momentum deposition to higher latitudes, will be quantitatively elucidated by the PANSY radar in combination with satellite and model data. Collaboration with the radars at other stations such as the ST radar at Davis station (Australia) is also important when examining the locality of wave characteristics.

3.3. Polar mesosphere summer echoes (PMSE) and polar mesospheric clouds (PMC)

Another interesting topic is clouds in the polar middle atmosphere, in particular, PMC. It is well known that a strong coherent echoes (PMSE) are observed from the polar summer mesosphere in association with PMC (von Zahn and Bremer, 1999; Klekociuk et al., 2008). The PMSE appear mainly above the PMC. The first PMSE observation in the Antarctic was performed by Woodman et al. (1999) at Machu-Picchu Station. They reported that the PMSE were significantly lower than those in the Arctic. However, subsequent radar observations at Davis and Wasa Stations in the Antarctic show that the strength of PMSE depends on the location, and that they are not necessarily weaker than those observed in the Arctic (Kirkwood et al., 2007; Latteck et al., 2007). In terms of the dominant height and onset, the PMSE in the Antarctic exhibit larger regional and interannual variabilities than those observed in the Arctic (e.g., Morris et al., 2012). Hoffmann et al. (2008) indicated a possible role of tides and gravity waves in the layered structure of PMSE. Theoretical studies on PMSE were reviewed by Cho and Roettger (1997) and Rapp and Luebken (2004). These echoes are considered to be related to ionization and the small-scale structure associated with PMC. The physical mechanism causing the inter-hemispheric variability of PMC was examined using a general circulation model (GCM) that included mesospheric chemistry and water vapor transport (e.g., Luebken and Berger, 2007).

In addition to PMSE, the PANSY radar can detect echoes from turbulence in the mesosphere. Thus, 3D winds can be estimated regardless of the presence of PMC. A Rayleigh lidar that was co-located at Syowa Station in early 2011, together with the PANSY radar, will be useful in clarifying the structure and evolution of PMC/PMSE over the Antarctic. Imaging observations using the PANSY radar will allow the 3D fine structure of PMSE and turbulence to be elucidated. A similar observational project started at Andoya, Norway, in the Arctic using Middle Atmosphere Alomar Radar System (MAARSY) (Latteck et al., 2012). The comparison of PMC characteristics in the Antarctic and Arctic atmosphere should be interesting. Recent studies (Becker and Fritts, 2006; Karlsson et al., 2009) have shown a possible link between the two hemispheres.

3.4. Coupling processes of the neutral atmosphere, ionosphere, and magnetosphere

The ionospheric observation of the PANSY radar will also reveal the inter-hemispheric differences of the coupling process between the atmosphere and the magnetosphere. The recent observations by satellites have shown that the field-aligned currents from the magnetosphere have strong inter-hemispheric differences that cannot be explained by the magnetospheric processes alone, but by the coupling processes between the atmosphere and the magnetosphere (Clausen et al., 2012). There are several observations that imply the inter-hemispheric difference of the energy input from the magnetosphere to the ionosphere (Tsugawa et al., 2006). The sources of the energetic particles that make the auroral emission, and the field-aligned currents that make the Joule heating in the ionosphere, are supposed to be on the equatorial plane in the magnetosphere, and not to have the inter-hemispheric asymmetry. Therefore it is suggested that the inter-hemispheric differences are caused by the differences of the density, temperature and composition of the atmosphere between the hemispheres. These differences make the different coupling between the magnetosphere and the atmosphere. Because the ground-based facilities designed to observe the ionosphere are concentrated in the northern hemisphere, and because there is no incoherent scatter radar in the Antarctica, ionospheric observations of the PANSY radar can be expected to contribute to efforts aimed at clarifying the coupling processes between the atmosphere and the solar wind through the magnetosphere.

3.5. Improvement of climate prediction models

Global models for weather prediction and climate projection with relatively low resolution still have a cold bias in the winter polar stratosphere and unrealistic timing of the final warming in the stratosphere. It is considered likely that this is at least partly due to unrealistic gravity wave parameterizations. This bias

significantly degrades the predictions of the Antarctic ozone hole and ozone layer recovery, because stratospheric temperature affects PSC volume (e.g., McLandress et al., 2012). Moreover, Cagnazzo and Manzini (2009) recently reported that climate models with a low top (in the middle stratosphere) are not able to simulate realistic sea level pressures and temperatures in the Arctic associated with El Nino events in the tropics, while high-top models that include the whole stratosphere and mesosphere can. This fact indicates that the middle atmosphere significantly affects the surface climate. Quantitative understandings of polar atmospheric dynamics made possible by adding the PANSY radar to the current observational network, in combination with higher-resolution GCMs, can be expected to reduce such model biases and contribute to the improvement of climate prediction.

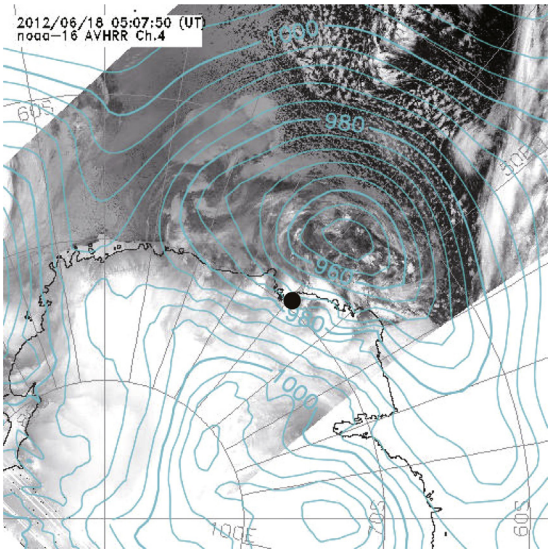

Fig. 6. A satellite infrared image at 8:07 50″ LST (05:07 50″ UTC) on July 18, 2012, overlaid with a sea level pressure map at 9:00 LST (03:00 UTC), when a Class B blizzard was recorded at Syowa Station. The black circle denotes the location of Syowa Station.

4. Preliminary results

4.1. Observation of a severe snow storm in the troposphere and stratosphere

Since the end of April 2012, troposphere/lower stratosphere observations have been performed almost continuously with the radar system operating 12 subarrays (228 antennas). Echo power spectra taken at one minute intervals were analyzed by an offline fitting program (Sato et al., 1997), which gives robust and accurate estimates of the echo power, line-of-sight velocity, and spectral width, even under noisy conditions for which conventional real-time fitting programs may fail. 3D winds were then estimated from the line-of-sight velocities during several severe snow using five beams oriented to the vertical, northward, eastward, southward and westward at zenith angles of 10°. The range resolution was set at 150 m. In this section, we show some results from the analysis of the PANSY radar observation data for the time period from June 15, 00:00 UTC to June 20, 2012, 00:00 UTC including two class-B blizzard periods: from June 15, 19:00 UTC to June 16, 20:05 UTC, and from June 17, 17:20 UTC to June 18, 2012, 11:20 UTC.

Fig. 6 shows an infrared (IR) satellite map taken at 05:07:50 UTC on June 18, 2012, overlaid with contours of sea level pressure at 06:00 UTC on June 18, 2012, from the Modern Era-Retrospective

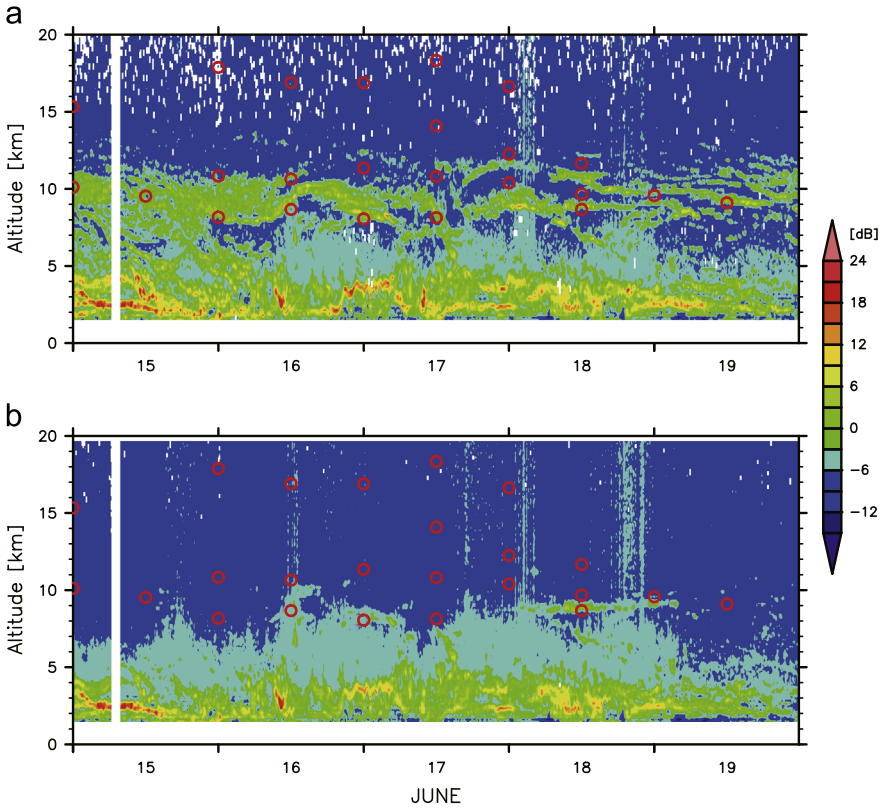

Fig. 7. Height–time sections of echo power observed by (a) the vertical beam and (b) average of four oblique beams of the PANSY radar when Syowa Station was hit by the Class B blizzard shown in Fig. 6. The circles denote the tropopause as determined by twice daily operational radiosonde observations conducted by the Japan Meteorological Agency at Syowa Station. (For interpretation of the references to color in this figure legend, the reader is referred to the web version of this article.)

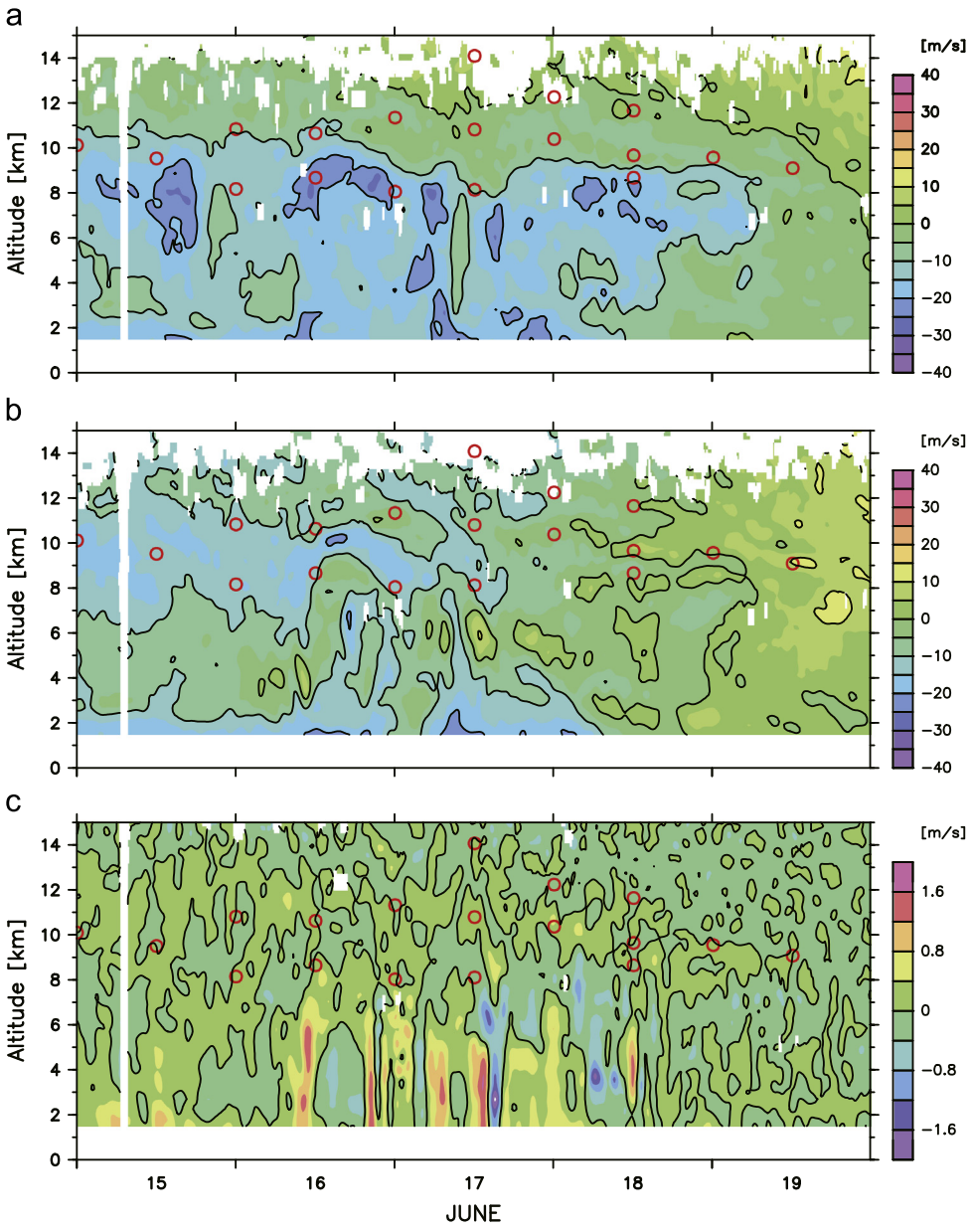

Fig. 8. Same as Fig. 7, but for (a) zonal, (b) meridional and (c) vertical winds observed by the PANSY radar at Syowa Station. The contour intervals are 10 m s^{-1} for zonal and meridional winds. Only contours of 0 m s^{-1} are shown for vertical winds. Smoothing was performed using low-pass filters with a cutoff length of 1 km in the vertical and of 2 h in time.

Analysis for Research and Applications (MERRA) (Rienecker et al., 2011). The closed circle denotes the location of Syowa Station. A strong cyclone with a minimum pressure of 955 hPa is situated to the north of Syowa Station, although clouds are not clearly discernible as in mature tropical cyclones.

The time–height sections of the echo power observed by the vertical beam and an average of observations by four oblique beams are shown in Fig. 7a and b, respectively. Tick marks of the horizontal axis show 00:00 UTC of each day. The echoes detected by the vertical beam are primarily from atmospheric turbulence and partial reflection due to static stability, while that by oblique beams are mainly due to atmospheric turbulence. The difference between the two echo plots shown in Fig. 7a and b indicates the existence of strong echo layers in a height range of 7–13 km for the vertical beam. Red circles denote the tropopause defined by the World Meteorological Organization using operational radiosonde observations made by the Japan Meteorological

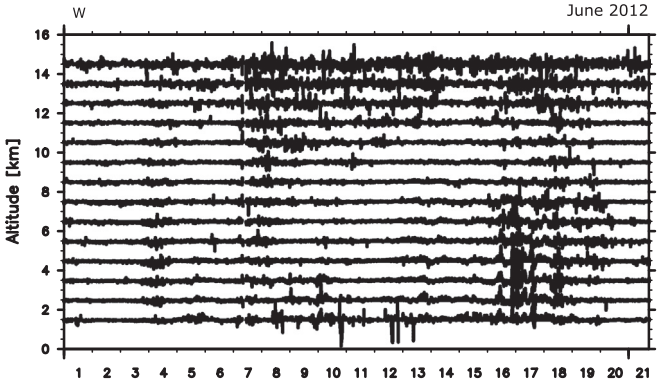

Fig. 9. Time series of unfiltered vertical winds in the time period of June 1–21, 2012, at a 1.5–14.5 km height region and with a 1 km interval. The vertical length of adjacent horizontal lines corresponds to 3 m s^{-1}.

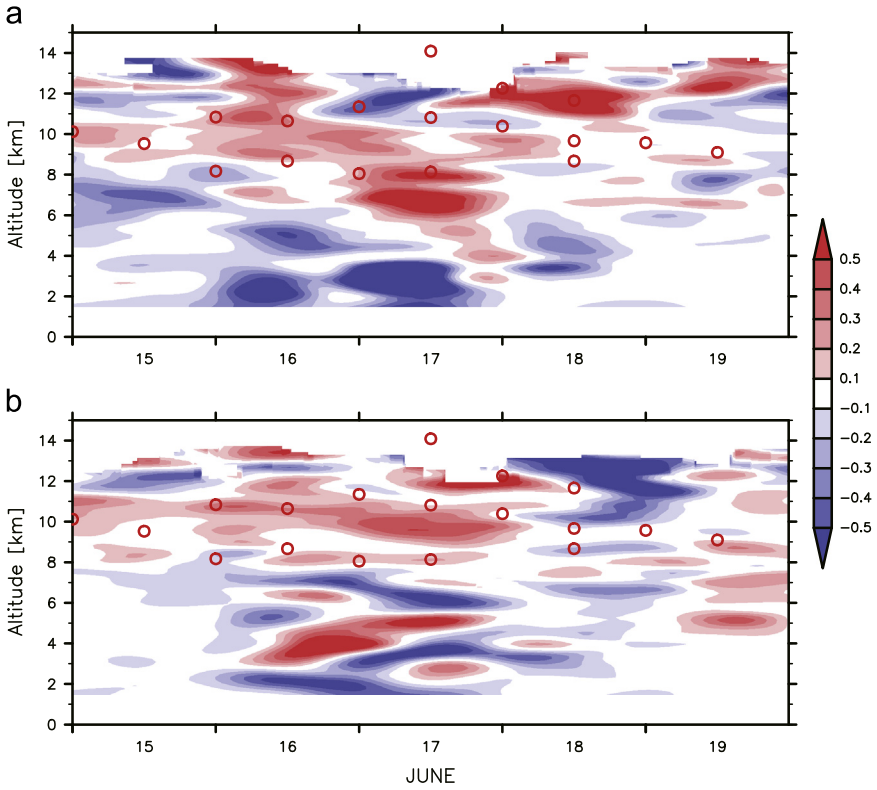

Fig. 10. Same as Fig. 7, but for vertical fluxes of (a) zonal and (b) meridional momentum associated with fluctuation components with periods shorter than 13 h which is the inertial period at Syowa Station (69°S).

Agency at Syowa Station. By the definition, the second or more tropopauses were detected. It is clear that the lower ends of the strong echo layers in 7–13 km correspond to the tropopause. Temporal variation in the strong echo layers is quite dynamic, suggesting possible stratosphere-troposphere exchange. Mihalikova et al. (2012), Arnault and Kirkwood (2012) and Alexander et al. (2013) examined the structure and variability of the tropopause using radar echo power measurements at Wasa and Davis Stations, respectively. Moreover, it is also interesting to examine such the fine structure around the tropopause in terms of the simultaneous occurrence of the PSC and upper tropospheric (or tropopausal) clouds (Kohma and Sato, 2013). We expect that, when fully online, the PANSY radar system will be able to detect stratospheric echoes up to a height of about 24 km.

Horizontal wind components are obtained by line-of-sight velocities estimated by oblique beam observations. The line-of-sight velocities estimated by vertical beam observation are shown as the vertical wind component. Time–height sections of zonal (eastward) (u), meridional (northward) (v), and vertical (w) wind components are shown in Fig. 8. Plotted winds were smoothed by lowpass filters with cutoff length of 2 h in time and 1 km in the vertical. During the analyzed time period, the zonal wind is mainly westward in the troposphere, while mean meridional wind is weak. This feature is consistent with the horizontal map of sea level pressure shown in Fig. 6. Strong upward and downward winds extending to the whole troposphere are observed on June 16, 08:00 UTC to June 18, 18:00 UTC. Corresponding structures are observed also in the zonal and meridional winds (Fig. 8a and b).

The time series of unfiltered vertical winds over the time period of June 1–21, 2012, are plotted at each height in Fig. 9. During this time period, four blizzards including those shown in Figs. 7 and 8 occurred. Two others occurred from June 8, 18:00 UTC to June 9, 16:45 UTC (Class C) and from 09:00 to 16:40 UTC on June 10, 2012 (Class B). The vertical length of the adjacent horizontal lines corresponds to wind speeds of 3 m s^{-1}. As can be seen in the figures, the vertical wind fluctuations were extremely strong in the troposphere from June 16 to June 18. The magnitude of the upward and downward winds amounts to a few meter per seconds. Strong vertical wind disturbances are also observed in the stratosphere from June 16 to June 18, although similar stratospheric disturbances are seen from June 7 to June 14. These strong vertical wind fluctuations seem to be connected to the disturbances in the troposphere. An interesting feature is that the time scales of the vertical wind fluctuations in the troposphere seem to be longer than those in the lower stratosphere. The existence of similar short-period vertical wind fluctuations in the stratosphere associated with cyclones was reported by Sato (1993) in relation to the MU radar observations of a typhoon.

Fig. 10 shows momentum fluxes associated with fluctuation components with periods shorter than 13 h, which is the inertial period at Syowa Station (69°S). The method devised by Vincent and Reid (1983) was used for the estimation. Smoothing was made with a lowpass filter with a cutoff length of 1 km in the vertical and a lowpass filter with a time cutoff length of 24 h, which roughly corresponds to a running mean with a length of 12 h, so as to see the overall structure easily. In the June 16–17 time period when strong vertical disturbances were observed, $\overline{u'w'}$ is strongly negative in the lower troposphere, while it is strongly positive in the upper troposphere on June 17. In the lower stratosphere, both $\overline{u'w'}$ and $\overline{v'w'}$ are generally positive from 8 to 10 km in the time period of June 15–17, while both positive and negative values are observed in other regions and days.

Fig. 11 is the same as Fig. 10 but for fluctuation components with periods shorter than 1 h. Note that only this type of radar can examine such high frequency component. Large momentum flux values are not seen in the troposphere, except for negative $\overline{u'w'}$ in the upper troposphere, while large magnitude values are seen in both $\overline{u'w'}$ and $\overline{v'w'}$ in the lower stratosphere. This fact indicates

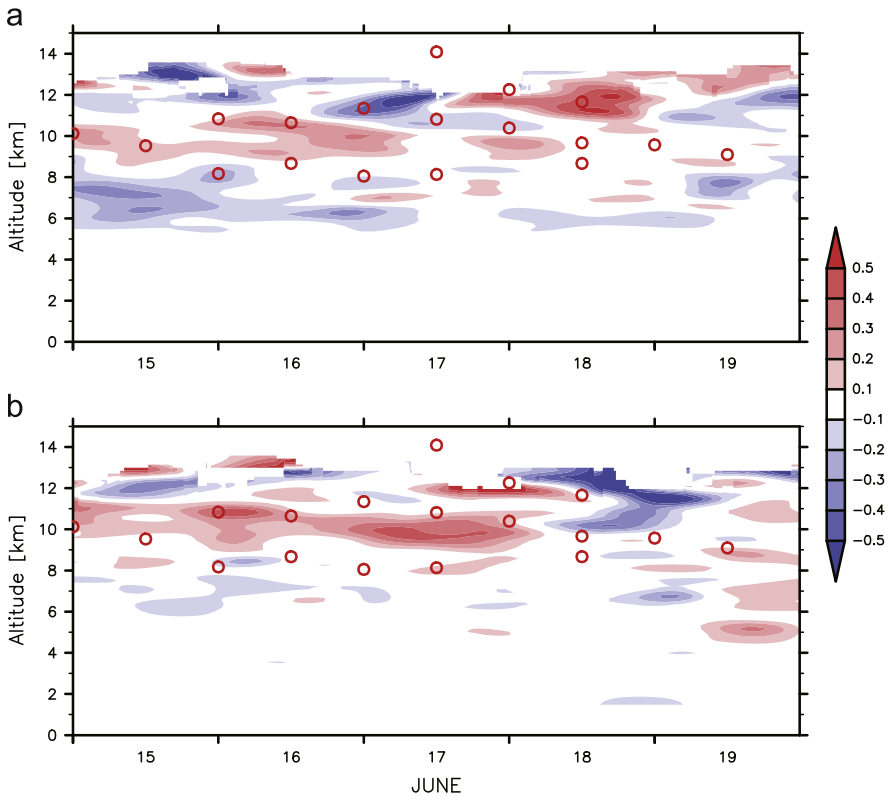

Fig. 11. Same as Fig. 10, but for fluctuations with periods shorter than 1 h.

that the momentum fluxes observed in the troposphere in Fig. 10 are primarily due to components with periods longer than 1 h, while a significant part of momentum fluxes in the lower stratosphere are associated with components that have periods shorter than 1 h. These wind disturbances with significant momentum fluxes in the stratosphere are likely due to internal gravity waves.

Because PANSY radar observations are limited at a single location, studies utilizing a combination of numerical simulations will be needed for further physical interpretation of these phenomena. However, this is beyond scope of the present paper and will be left for future studies.

4.2. *Observation of polar mesosphere summer echo (PMSE)*

During summer time operation at Syowa Station in early 2012, we observed PMSE with one subarray (19 antennas) using five beams pointing to the vertical, north, east, south, and west at the same zenith angle of 10°. The two-way half-power beam width of this experiment is 13°. The range resolution is 600 m. For the time period from January 6 to February 5, 2012 when significant echoes were detected from the mesosphere, the occurrence frequency of PMSE was calculated as a function of local time for each range. Following Kirkwood et al. (2007), PMSE were defined as the echoes with volume reflectivity greater than 1×10^{-15} m^{-1}. As the sensitivity of the radar system used for this observation was not sufficient for this criterion, we selected echoes with volume reflectivity greater than 1×10^{-14} m^{-1}.

The results are shown in Fig. 12 where contours of values greater than 6% are drawn at an interval of 4%. Here, it can also be seen that PMSE are mainly observed around a height of 85 km (Fig. 12a), which is consistent with previous studies (e.g., Latteck et al., 2007; Kirkwood et al., 2008). It is clear that there is strong local time dependence. There are two peaks around 07:00 LT and 14:00–18:00 LT. This diurnal variation in the occurrence frequency is consistent with the observations taken at Andenes and Davis Stations (Morris et al., 2009). The diurnal variation can be affected by temperature modulation by tides and latitudinal transport of cold air from the high latitudes (Hoffmann et al., 1999). The stronger peak around 07:00 LT is observed after equatorward flow associated with tides is maximized at Syowa Station. The relative strength and/or local time of the two peaks, however, depend on year and geographical location. Thus, further studies on the diurnal variation are needed.

Figs. 12b and 12c show the local time and range sections of PMSE occurrence frequency detected by oblique beams. The timing of large occurrence frequency of PMSE is similar among the four beams. However, it appears that the upper end of the ranges where PMSE are frequently detected depends on the beam direction. More specifically, it is higher for observations via the south (east) beam than via the north (west) beam. This feature suggests the possibility that PMSE have small-scale spatial structures which will need to be examined in detail in the future. Similar observations of the small-scale structures of PMSE in the Arctic were reported by Rapp et al. (2011) using multi-beam observations from the MAARSY.

5. Conclusion remarks

In this paper, we provided a description of the PANSY radar system, which is the first MST/IS radar constructed in the Antarctic, together with possible observation techniques. After briefly reviewing the construction history of the radar up to the present, we examined the radar system with an emphasis on the special considerations needed to match Antarctic environmental conditions, such as severe weather and resource limitations. We then described the state-of-the-art radio engineering techniques that were introduced to overcome those difficulties.

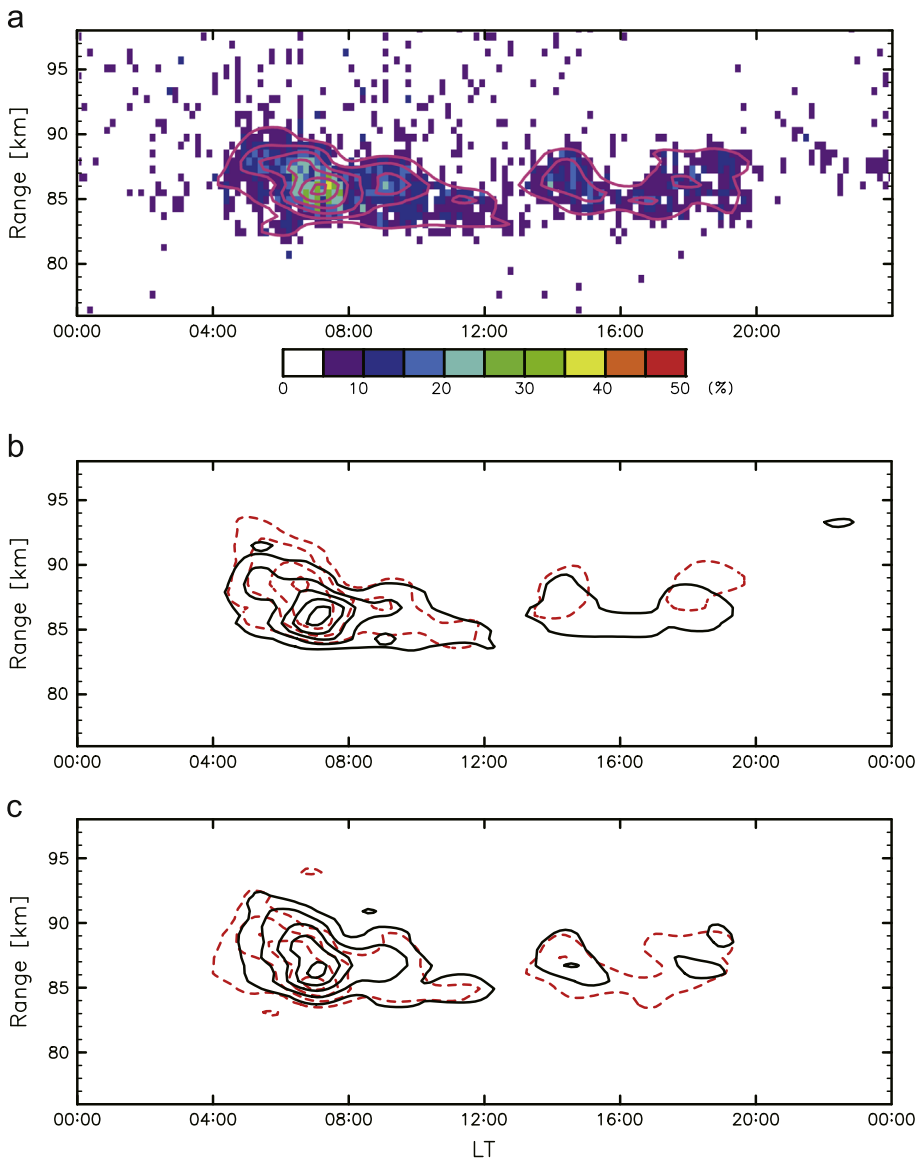

Fig. 12. Occurrence frequency distribution of PMSE in the height and local time section at (a) the vertical beam, (b) oblique beams in the N–S plane, and (c) oblique beams in the E–W plane. The contours of values greater than 6% are drawn at an interval of 4%. The dashed contours in (b) and (c) indicate the south and the west beams, respectively.

Next, we discussed the scientific targets of the PANSY radar with a short review of recent related studies. By making full use of its ability to continuously monitor the wind, turbulence, and ionospheric parameters with high time and height resolutions, we can study various phenomena characteristic to the Antarctic region in detail. Such studies will include convection associated with synoptic-scale cyclones/polar lows, gravity waves in the troposphere, stratosphere, mesosphere, and ionosphere, as well as ionospheric disturbances, and auroral events. Based on the long term data, important issues related to Antarctic atmospheric science, such as the unique clouds in the polar region (PSC and PMC), the interaction of katabatic winds with cyclones, stratosphere–troposphere exchange, the effects of the continent on the upper atmosphere, dynamical coupling in the vertical of the whole atmosphere and inter-hemispheric coupling through the mesosphere and stratosphere are expected to be clarified.

Finally, we presented and discussed the preliminary results of our initial observations. Using a partial system consisting of 228 antennas, interesting phenomena such as vertical wind disturbances (possibly due to active gravity waves) having significant momentum fluxes and temporal variations in multiple tropopauses which are associated with severe snow storms were found from a continuous observation taken over a one-month period. Moreover, even with the smallest system consisting of a 19-antenna subarray, important features of PMSE that are consistent with previous studies were observed.

Acknowledgments

The PANSY project started in 2000 and the radar construction was made in 2009. We are indebted to Profs./Drs. Masaki Ejiri and Takehiko Aso for their continuous advice in performing this major project. We greatly appreciate Profs. Susumu Kato, Shoichiro Fukao, Ronald Woodman, Juergen Roettger, Isamu Hirota, Marvin Geller, Kevin Hamilton, Robert R. Vincent, and Yoshiyuki Fujii as well as many other scientists for their continuous and strong encouragements. Mr. Masahiro Nomoto created a figure. See the PANSY program website for details: http://pansy.eps.s.u-tokyo.ac.jp.

References

Alexander, M.J., et al., 2008. Global estimates of gravity wave momentum flux from high resolution dynamics limb sounder observations. Journal of Geophysical Research 113, D15S18, 10.1029/2007JD008807.

Alexander, M.J., Eckermann, S.D., Broutman, D., Ma, J., 2009. Momentum flux estimates for South Georgia Island mountain waves in the stratosphere observed via satellite. Geophysical Research Letters 36, L12816.

Alexander, M.J., et al., 2010. Recent developments in gravity-wave effects in climate models and the global distribution of gravity-wave momentum flux from observations and models. Quarterly Journal of the Royal Meteorological Society 136, 1103–1124.

Alexander, S.P., Murphy, D.J., Klekociuk, A.R., 2013. High resolution VHF radar measurements of tropopause structure and variability at Davis, Antarctica (69°S, 78°E). Atmospheric Chemistry and Physics 13, 3121–3132.

Arnault, J., Kirkwood, S., 2012. Dynamical influence of gravity waves generated by the Vestfjella Mountains in Antarctica: radar observations, fine-scale modelling and kinetic energy budget analysis. Tellus A 64, 17261, http://dx.doi.org/10.3402/tellusa.v64i0.17261.

Becker, E., Fritts, D.C., 2006. Enhanced gravity wave activity and interhemispheric coupling during the MaCWAVE/MIDAS northern summer program 2002. Annales Geophysicae 24, 1175–1188.

Bowhill, S.A., 1983. Foreword: Workshop on technical aspects of MST radar, May 23–27, 1983. Handbook for MAP 9, iii.

Bromwich, D.H., Steinhoff, D.F., Simmonds, I., Keay, K., Fogt, R.L., 2011. Climatological aspects of cyclogenesis near Adélie Land Antarctica. Tellus A 63, 921–938, http://dx.doi.org/10.1111/j.1600-0870.2011.00537.x.

Cagnazzo, C., Manzini, E., 2009. Impact of the stratosphere on the winter tropospheric teleconnections between ENSO and the North Atlantic and European region. Journal of Climate 22, 1223–1238.

Cho, J.Y.N., Roettger, J., 1997. An updated review of polar mesosphere summer echoes: observation, theory, and their relationship to noctilucent clouds and subvisible aerosols. Journal of Geophysical Research 102, 2001–2020.

Clausen, L.B.N., Baker, J.B.H., Ruohoniemi, J.M., Milan, S.E., Anderson, B.J., 2012. Dynamics of the region 1 Birkeland current oval derived from the Active Magnetosphere and Planetary Electrodynamics Response Experiment (AMPERE). Journal of Geophysical Research 117, A06233, http://dx.doi.org/10.1029/2012JA017666.

Ern, M., Preusse, P., Alexander, M.J., Warner, C.D., 2004. Absolute values of gravity wave momentum flux derived from satellite data. Journal of Geophysical Research 109, D20103, http://dx.doi.org/10.1029/2004JD004752.

Fukao, S., et al., 1979. Mesospheric winds and waves over Jicamarca on May 23–24, 1974. Journal of Geophysical Research 84, 4379–4386.

Fukao, S., et al., 1985. The MU radar with an active phased array system, 1. Antenna and power amplifiers. Radio Science 20, 1155–1168.

Gage, K.S., Balsley, B.B., 1978. Doppler radar probing of the clear atmosphere. Bulletin of American Meteorological Society 59, 1074–1093.

Geller, M.A., et al., 2013. A comparison between gravity wave momentum fluxes in observations and climate models. Journal of Climate 26, 6383–6405 10.1175/JCLI-D-12-00545.1.

Hocking, W.K., 1985. Measurement of turbulent energy dissipation rates by radar techniques: a review. Radio Science 20, 1403–1422.

Hoffmann, P., Singer, W., Bremer, J., 1999. Mean seasonal and diurnal variations of PMSE and winds from 4 years of radar observations at ALOMAR. Geophysical Research Letters 26, 1525–1528.

Hoffmann, P., Rapp, M., Fiedler, J., Latteck, R., 2008. Influence of tides and gravity waves on layering processes in the polar summer mesopause region. Annales Geophysicae 26, 4013–4022.

Karlsson, B., McLandress, C., Shepherd, T.G., 2009. Inter-hemispheric mesospheric coupling in a comprehensive middle atmosphere model. Journal of Atmospheric and Solar–Terrestrial Physics 41, 518–530.

Kero, J., et al., 2012. A meteor head echo analysis algorithm for the lower VHF band. Annales Geophysicae 30, 639–659.

Kirkpatrick, S., Gelatt, C.D., Vecchi, M.P., 1983. Optimization by simulated annealing. Science, New Series 220, 671–680.

Kirkwood, S., et al., 2007. Polar mesosphere summer echoes at Wasa, Antarctica (73°S): First observations and comparison with 68°N. Geophysical Research Letters 34, L15803, http://dx.doi.org/10.1029/2007GL030516.

Kirkwood, S., et al., 2008. A new height for the summer mesopause: Antarctica, December 2007. Geophysical Research Letters 35, L23810, http://dx.doi.org/10.1029/2008GL035915.

Klekociuk, A.R., Morris, R.J., Innis, J.L., 2008. First Southern Hemisphere common-volume measurements of PMC and PMSE. Geophysical Research Letters 35, L24804, http://dx.doi.org/10.1029/2008GL035988.

Kohma, M., Sato, K., 2013. Simultaneous occurrence of polar stratospheric clouds and upper-tropospheric clouds caused by blocking anticyclones in the Southern Hemisphere. Atmospheric Chemistry and Physics 13, 3849–3864, http://dx.doi.org/10.5194/acp-13-3849-2013.

Latteck, R., et al., 2007. Observation of polar mesosphere summer echoes with calibrated VHF radars at 69° in the Northern and Southern hemispheres. Geophysical Research Letters 34, L14805, http://dx.doi.org/10.1029/2007-GL030032.

Latteck, R., et al., 2012. MAARSY: the new MST radar on Andøya-System description and first results. Radio Science 47, RS1006, http://dx.doi.org/10.1029/2011RS004775.

Luebken, F.-J., Berger, U., 2007. Interhemispheric comparison of mesospheric ice layers from the LIMA model. Journal of Atmospheric and Solar–Terrestrial Physics 69, 2292–2308.

McLandress, C., Shepherd, T.G., Polavarapu, S., Beagley, S.R., 2012. Is missing orographic gravity wave drag near 60°S the cause of the stratospheric zonal wind biases in chemistry-climate models? Journal of the Atmospheric Sciences 69, 802–818.

Mihalikova, M., Kirkwood, S., Arnault, J., Mikhaylova, D., 2012. Observation of a tropopause fold by MARA VHF wind-profiler radar and ozonesonde at Wasa, Antarctica: comparison with ECMWF analysis and a WRF model simulation. Annales Geophysicae 30, 1411–1421.

Morris, R.J., Murphy, D.J., Reid, I.M., Holdsworth, D.A., Vincent, R.A., 2004. First polar mesosphere summer echoes observed at Davis, Antarctica (68.6°S). Geophysical Research Letters 31, L16111, http://dx.doi.org/10.1029/2004GL020352.

Morris, R.J., et al., 2009. Inter-hemispheric asymmetry in polar mesosphere summer echoes and temperature at 69o latitude. Journal of Atmospheric and Solar–Terrestrial Physics 71, 464–469.

Morris, R.J., Klekociuk, A.R., Holdsworth, D.A., 2011. First observations of Southern Hemisphere polar mesosphere winter echoes including conjugate occurrences at ~69°S latitude. Geophysical Research Letters 38, L03811, http://dx.doi.org/10.1029/2010GL046298.

Morris, R.J., et al., 2012. Experimental evidence of a stratospheric circulation influence on mesospheric temperatures and ice-particles during the 2010–2011 austral summer at 69°S. Journal of Atmospheric and Solar–Terrestrial Physics 89, 54–61.

Nakamura, T., et al., 1991. Meteor wind observations with the MU radar. Radio Science 26, 857–869.

Nakamura, T., et al., 1997. Studies of the MLT region using the MU radar and simultaneous observations with OH spectrometer and other optical instruments. Advances in Space Research 19, 643–652.

Nishimura, K., Sato, T., Nakamura, T., Ueda, M., 2001. High sensitivity radar-optical observations of faint meteors. IEICE Transactions on Communications E84-C, 1877–1884.

Rapp, M., Luebken, F.-J., 2004. Polar mesosphere summer echoes (PMSE): review of observations and current understanding. Atmospheric Chemistry and Physics 4, 2601–2633.

Rapp, M., et al., 2011. First three-dimensional observations of polar mesosphere winter echoes: resolving space-time ambiguity. Journal of Geophysical Research 116, A11307, http://dx.doi.org/10.1029/2011JA016858.

Rienecker, M.M., et al., 2011. MERRA—NASA's modern-era retrospective analysis for research and applications. Journal of Climate 24, 3624–3648.

Roettger, J., Rastogi, P.K., Woodman, R.F., 1979. High-resolution VHF radar observation of turbulent structures in the mesosphere. Geophysical Research Letters 8, 617–620.

Sato, K., 1993. Small-scale wind disturbances observed by the MU radar during the passage of Typhoon Kelly. Journal of the Atmospheric Sciences 50, 518–537.

Sato, K., O'Sullivan, D.J., Dunkerton, T.J., 1997. Low-frequency inertia-gravity waves in the stratosphere revealed by three-week continuous observation with the MU radar. Geophysical Research Letters 24, 1739–1742.

Sato, K., Hirasawa, N., 2007. Statistics of Antarctic surface meteorology based on hourly data in 1957–2007 at Syowa Station. Polar Science 1, 1–15.

Sato, K., et al., 2009. On the origins of gravity waves in the mesosphere. Geophysical Research Letters 36, L19801, http://dx.doi.org/10.1029/2009GL039908.

Sato, K., Tateno, S., Watanabe, S., Kawatani, Y., 2012. Gravity wave characteristics in the Southern Hemisphere revealed by a high-resolution middle-atmosphere general circulation model. Journal of the Atmospheric Sciences 69, 1378–1396 10.1175/JAS-D-11-0101.1.

Sato, T., et al., 1985. High-resolution MST observations of turbulence by using the MU radar. Radio Science 20, 1452–1460.

Sato, T., et al., 1989. Ionospheric incoherent scatter measurements with the middle and upper atmosphere radar: techniques and capability. Radio Science 24, 85–98.

Sato, T., Nakamura, T., Nishimura, K., 2000. Orbit determination of meteors using the MU radar. IEICE Transactions on Communications E83-B, 1990–1995.

Spano, E., Ghebrebrhan, O., 1996. Pulse coding techniques for ST/MST radar systems: a general approach based on a matrix formulation. IEEE Transaction on Geoscience and Remote Sensing 34, 304–316.

Thomas, G.E., Olivero, J.J., Deland, M., Shettle, E.P.P., 2003. Comment on "Are noctilucent clouds truly a "Miner's Canary" for Global Change?". Eos, Transactions American Geophysical Union 84, 352–353, http://dx.doi.org/10.1029/2003EO360008.

Tsugawa, T., et al., 2006. Geomagnetic conjugate observations of large-scale traveling ionospheric disturbances using GPS networks in Japan and Australia. Journal of Geophysical Research 111, A02302, http://dx.doi.org/10.1029/2005JA011300.

Tsutsumi, M., Tsuda, T., Nakamura, T., Fukao, S., 1994. Temperature fluctuations near the mesopause inferred from meteor observations with the middle and upper atmosphere radar. Radio Science 29, 599–610.

Tsutsumi, M., Tsuda, T., Nakamura, T., Fukao, S., 1996. Wind velocity and temperature fluctuations due to a 2-day wave observed with radio meteor echoes. Journal of Geophysical Research 101, 9425–9432.

Vincent, R.A., Reid, I.M., 1983. HF Doppler measurements of mesospheric gravity wave momentum fluxes. Journal of the Atmospheric Sciences 40, 1321–1333.

von Zahn, U., 2003. Are noctilucent clouds a "Miner's Canary" for global change? Eos, Transactions, American Geophysical Union 84, 261–264, http://dx.doi.org/10.1029/2003EO280001.

von Zahn, U., Bremer, J., 1999. Simultaneous and common-volume observations of noctilucent clouds and polar mesosphere summer echoes. Geophysical Research Letters 26, 1521–1524.

Watanabe, S., et al., 2008. General aspects of a T213L256 middle atmosphere general circulation model. Journal of Geophysical Research 113, D12110, http://dx.doi.org/10.1029/2008JD010026.

Woodman, R.F., et al., 1999. First observations of polar mesosphere summer echoes in Antarctica. Journal of Geophysical Research 104, 22577–22590.

Yoshiki, M., Sato, K., 2000. A statistical study of gravity waves in the polar regions based on operational radiosonde data. Journal of Geophysical Research 105, 17995–18011.